TACC3–ch-TOG track the growing tips of microtubules independently of clathrin and Aurora-A phosphorylation

Cristina Gutiérrez-Caballero[1], Selena G. Burgess[2,3], Richard Bayliss[2,3] & Stephen J. Royle[1]*

[1] Division of Biomedical Cell Biology, Warwick Medical School, Gibbet Hill Road, Coventry, CV4 7AL, UK

[2] Department of Biochemistry, University of Leicester, Leicester LE1 9HN, UK

[3] Cancer Research UK Leicester Centre, UK

* Author for correspondence

+44 247651931

s.j.royle@warwick.ac.uk

Abstract

The interaction between TACC3 (transforming acidic coiled coil protein 3) and the microtubule polymerase ch-TOG (colonic, hepatic tumor overexpressed gene) is evolutionarily conserved. Loading of TACC3–ch-TOG onto spindle microtubules requires the phosphorylation of TACC3 by Aurora-A kinase and the subsequent interaction of TACC3 with clathrin to form a microtubule binding surface. Whether there is a pool of TACC3–ch-TOG that is independent of clathrin in human cells, and what is the function of this pool, are open questions. Here, we report that TACC3 is recruited to the plus-ends of microtubules by its association with ch-TOG and that this pool is independent of phosphorylation and binding to clathrin. The plus-end binding of TACC3–ch-TOG persists in interphase and we propose that one cellular function of TACC3–ch-TOG is to modulate cell migration. We also describe the distinct subcellular pools of TACC3, ch-TOG and clathrin. TACC3 is often described as a centrosomal protein, but we show that there is no significant population of TACC3 at centrosomes. The delineation of distinct protein pools reveals a simplified view of how these proteins are organized and controlled by post-translational modification.

Introduction

Microtubules (MTs) are dynamic polymers of α/β-tubulin that are involved in numerous cellular processes, including intracellular transport, chromosome segregation and control of cell shape and migration. Each MT is polarized, having a fast-growing plus-end and a minus-end that grows more slowly. The plus-ends swap between episodes of growth and shrinkage, powered by GTP hydrolysis [1]. MT plus-end tracking proteins (+TIPs) bind the plus-ends of MTs, typically during episodes of growth [2].

Among the best-known +TIPs are the end-binding (EB) proteins (EB1-3) and proteins with TOG or TOG-like domains, e.g. ch-TOG/XMAP215 [3, 4]. EB proteins can recruit a plethora of proteins, mainly via [ST]X[IL]P motifs, to induce their plus-end tracking behavior [5]. An exception is ch-TOG/XMAP215 which contains no [ST]X[IL]P motifs [6] and tracks plus ends *ahead* of EB proteins [7-9]. EB proteins and ch-TOG have different modes of binding. EB proteins bind growing ends of MTs, but do not select between plus and minus ends, whereas ch-TOG/XMAP215 only binds the plus-ends but does not distinguish between growing and shrinking ends [8, 9].

Transforming acidic coiled-coil protein 3 (TACC3) is a cancer-associated protein that binds ch-TOG [10]. The interaction is evolutionarily conserved and occurs via a break in the coiled-coil (TACC) domain of TACC3 and a region C-terminal to the TOG6 domain on ch-TOG [11, 12]. TACC3–ch-TOG complexes were originally proposed to antagonize the function of the MT depolymerase KIF2C/MCAK at spindle poles [13] and stimulate MT assembly independently of MCAK [14]. TACC3 is a substrate of Aurora-A kinase, which phosphorylates TACC3 on serine 558 [13, 15, 16]. It is now clear that this phosphorylation permits TACC3 to bind clathrin heavy chain whereupon the TACC3–clathrin can bind MTs in concert [11, 17-20]. The ternary complex of TACC3–ch-TOG–clathrin is involved stabilizing kinetochore fibers of the mitotic spindle by inter-MT bridging [17]. This information, and the observation that removal of clathrin by knocksideways removes all TACC3 from the spindle cast doubt on whether a pool of TACC3–ch-TOG binary complex is present in mitotic cells [21]. Recently, two further roles for TACC3 at the mitotic spindle have recently been proposed: 1) in anaphase MT sliding [22] and 2) in acentrosomal MT assembly during prometaphase [23]. It is unclear if these functions are in concert with clathrin, ch-TOG or both.

An important goal is to now define what pools of these protein complexes and sub-complexes exist in mitotic cells and what their respective functions may be. For example, TACC3 is thought of as an adaptor protein that, together with clathrin, locates ch-TOG on spindle MTs [12, 24]. What is puzzling about the adaptor function of TACC3 is that ch-TOG has six TOG domains (which bind tubulin dimers) and a positively charged stretch of residues that binds the MT lattice [25, 26]. If ch-TOG is competent for MT association, then why does it need a TACC3–clathrin adaptor?

We set out to investigate these issues and define the subcellular locations of each protein, beginning by examining the dynamics of TACC3 on MTs. We discovered that a fraction of TACC3 behaves as a +TIP, with ch-TOG mediating the association of TACC3 with the MT plus-end. This subcomplex is distinct from the Aurora-A-phosphorylated form of TACC3 that associates with clathrin in the TACC3–ch-TOG–clathrin complex on K-fibers during mitosis. Using this information, we describe the pools of TACC3, ch-TOG and clathrin, alone and in combination at different stages of the cell cycle.

Results and discussion

TACC3 is a microtubule plus-end tracking protein

Fluorescence recovery after photobleaching (FRAP) experiments indicated that TACC3 was highly dynamic on mitotic MTs and that there may be a second MT-binding pool of TACC3 (Supplementary Figure 1). To investigate this new pool of TACC3 in more detail, we used live-cell spinning disk confocal microscopy of human cell lines expressing GFP-tagged TACC3. In interphase and mitotic cells, GFP-TACC3 formed clear comet-like structures that moved in a directed manner, suggesting that TACC3 could behave as a MT plus-end tracking protein (+TIP).

Figure 1 shows examples of TACC3 +TIP behavior (see also Movies 1-3). GFP-TACC3 was transiently expressed in retinal pigment epithelial cells (RPE1) stably expressing EB3-tdTomato (Fig 1A). In this cell line, EB3 tracked the growth of MT plus-ends as previously described [2, 27]. GFP-TACC3 was present at the very distal tip of the growing MT, ahead of the EB3 signal (Fig 1A). Plus-end tracking of GFP-TACC3 was clearest in interphase where long periods of MT growth were marked by a small punctum of GFP-TACC3 fluorescence. However, in contrast to EB3-tdTomato, GFP-TACC3 stayed at the tip of MTs as they underwent shrinkage (Fig 1A, arrow). In mitotic cells, the +TIP behavior of TACC3 was most clear on the astral MTs, again tracking the plus ends ahead of EB3 (Fig 1A). At metaphase, these signals were often difficult to discern against the fluorescence on the K-fibers of the spindle and plus-end tracking of TACC3 was much clearer at anaphase on astral and interpolar MTs in either HeLa or RPE1 cells (see below).

Was the +TIP activity of TACC3 an artifact of transient expression of GFP-TACC3? Although we only imaged cells expressing very low levels of GFP-TACC3 – because overexpression resulted in aggregation of TACC3 [28] and no discernable +TIP activity – we wanted to rule out the possibility that +TIP behavior was an artifact of over-expression. As an alternative, we imaged live HeLa Kyoto cells expressing TACC3-GFP from a BAC transgene [20]. This protein is expressed at close-to-endogenous levels by virtue of the endogenous promoter. Again, TACC3 tracking the growth of MT plus-ends could clearly be seen (Fig 1B). These experiments indicate that TACC3 is a +TIP in interphase and mitotic cells and this novel population of TACC3 provides an explanation for slow fraction B in the FRAP experiments (Supplementary Figure 1).

TACC3 +TIP behavior depends on its interaction with ch-TOG

TACC3 binds ch-TOG and it had previously been reported that ch-TOG binds the plus-ends of MTs [7]. We hypothesized that TACC3 binds to ch-TOG, rather than directly binding to the distal end of the MT itself. We next tested if TACC3 +TIP behavior was dependent on ch-TOG +TIP activity. As the depletion of ch-TOG severely disrupts mitotic MTs [17], we sought an

alternative strategy. In cells depleted of endogenous TACC3, we expressed GFP-tagged TACC3 deletion mutants that had previously been shown to be unable to bind ch-TOG [11]. No +TIP activity was seen at interphase or anaphase for two different mutants, Δ678-681 or Δ682-688. Both mutants were still able to localize to the mitotic spindle (Fig 2A) [11]. These results suggest that TACC3–ch-TOG complexes can track the plus-ends of MTs and that plus-end recognition is by ch-TOG and not TACC3.

End-binding proteins, such as EB1, recruit proteins to the growing tips of MTs by virtue of [ST]X[IL]P motifs. Although TACC3 has no [ST]X[IL]P motif, it was detected in a pull-down for GST-EB1 binding proteins, albeit with low confidence [6]. We used the knocksideways system [21] to test for an interaction *in situ* between TACC3 and endogenous EB1. TACC3-depleted HeLa cells expressing GFP-FKBP-TACC3 and PAGFP-MitoTrap were treated with rapamycin (200 nM) or DMSO (0.1%) as a control. Fig 2B shows that GFP-FKBP-TACC3 was rerouted to the mitochondria upon addition of rapamycin. Endogenous EB1, detected by immunofluorescence remained in comets despite the rerouting of TACC3 to mitochondria. For comparison, and to verify that the interaction between TACC3 and ch-TOG also occurs during interphase, we also examined the distribution of endogenous ch-TOG following TACC3 rerouting and found that ch-TOG was co-rerouted to mitochondria (Fig 2B). These observations are consistent with a model where TACC3–ch-TOG binds the plus-ends of MTs independently of EB1.

TACC3 +TIP behavior is independent of Aurora-A phosphorylation and subsequent interaction with clathrin

We next tested the hypothesis that TACC3–ch-TOG +TIP activity was separate from the TACC3–ch-TOG–clathrin inter-MT bridge complex. Formation of the TACC3–ch-TOG–clathrin complex depends on Aurora-A phosphorylation of S558 on TACC3, allowing a dileucine motif (566,567) to bind to the ankle of clathrin heavy chain. We previously showed that non-phosphorylatable TACC3(S558A) and a TACC3 mutant in which the dileucine motif had been mutated (LL566,567AA) were unable to bind clathrin and could not localize to the mitotic spindle [11]. Live-cell imaging of either of these mutants in HeLa or RPE1 cells depleted of endogenous TACC3 showed +TIP tracking comparable to wild type GFP-TACC3 in interphase and anaphase (Fig 2A). Since +TIP activity for TACC3 was observed in interphase, a time when 1) Aurora-A activity is low and 2) clathrin is not known to interact with TACC3, this suggests that TACC3 +TIP activity is independent of clathrin-binding and phosphorylation by Aurora-A.

Potential role for +TIP activity of TACC3 in interphase cell migration

What is the cellular function of TACC3 binding to ch-TOG at the plus-ends of MTs? Analysis of this novel population of TACC3 was not possible during mitosis, because depleting or mutating TACC3 interferes with its role in stabilizing K-fibers as part of the TACC3–ch-TOG–clathrin complex. During interphase however, this complex is not formed and no mitotic spindle is

present; we therefore reasoned that this stage of the cell cycle was the best time to investigate the cellular function of TACC3 +TIP activity. RPE1 cells transfected with siRNAs targeting GL2 (control) or TACC3 were plated on fibronectin-coated dishes and imaged over 6 h and their 2D migration observed (see Methods). TACC3-depleted cells moved more slowly than control cells and the cumulative distance that they migrated was on average less than the control population (Fig 3A, 3B). Aligning the individual migration tracks so that their end position was along the same axis, gave the impression that growth was more directed after TACC3 depletion, and that the cells made fewer turns (Fig 3C). However, this apparent effect could be explained by the lower migration speed in TACC3-depleted cells because the relation between distance migrated and displacement was not significantly different from the control group (Fig 3D). The migration speed for TACC3-depleted cells was on average ~30% lower than control cells (Fig 3E, 3F). These results suggest that loss of the +TIP population of TACC3 changes MT dynamics in a way that inhibits cell migration. We propose that this is the interphase function of the +TIP activity of TACC3–ch-TOG, which may explain a previous report of altered cellular invasion which correlated with TACC3 expression levels [29].

Distinct pools of TACC3, ch-TOG, clathrin

TACC3 is often described as a centrosomal protein, and more recently, as a centrosomal adaptor protein [10]. We reconsidered the accuracy of this description, based on our own and published observations. The evidence that TACC3 is present at centrosomes comes from two studies. First, TACC3 was observed at spindle poles in nocodazole-treated cells [28]. However, this treatment leaves MT remnants that the TACC3–ch-TOG–clathrin may bind to rather than directly at the centrosome. Second, an antibody raised against TACC3 phosphorylated at S558 recognized centrosomes [13]. Later work showed that this antibody simply detects centrosomes and not TACC3 [19]. The signal for TACC3 pS558 detected with a new antibody was found over the K-fibers and not at the centrosomes [19]. One further reason that TACC3 is known as a centrosomal protein is historical. Initial work on TACC3 focused on potential similarities with the TACC homologs of lower species, where the relevant cell biology had originally been investigated, and in which TACC is found at the centrosomes/spindle pole body [30-32]. [28]. More recently however, multiple studies have failed to show obvious localization of TACC3 at the centrosome in mitotic higher eukaryotic cells [11, 18, 19, 33].

Our discovery of a +TIP pool of TACC3, associated with ch-TOG, prompted us to re-examine the subcellular distributions of TACC3, ch-TOG and clathrin. The aim was to document the possible combinatorial pools of TACC3, ch-TOG and clathrin in cells in mitosis or interphase. In mitotic cells, besides the +TIP pool of TACC3–ch-TOG, TACC3 is present on the K-fibers together with clathrin and ch-TOG but is largely absent from centrosomes; ch-TOG is additionally located at the centrosomes and kinetochores and clathrin is additionally found in coated pits and vesicles (Fig 4A). In interphase, ch-TOG is again found at centrosomes while TACC3 is absent from the centrosome in the majority of cells (Fig 4A, 4B). In cells where TACC3 was in the vicinity of

pericentrin staining, the two signals did not overlap and TACC3 might be present on MTs here rather than the centrosomes themselves (Fig 4C). Since plus-ends of MTs originate at the centrosome/spindle pole, this might explain apparent localization of TACC3 at the centrosome that may have been previously observed (Fig 1).

We propose that there are four distinct pools of TACC3, ch-TOG and clathrin in mitotic cells and three pools in interphase (Fig 4D, 4E). A proposed nanoscale model for the two MT-binding pools is shown in Fig 4F. Since only a small fraction of TACC3 is found close to the centrosome for a short period of the cell cycle, we suggest that TACC3 should not be referred to as a centrosomal protein. Instead, because TACC3 is a multifunctional protein, we recommend that TACC3's role either as a +TIP or as a MT adaptor is used as a definition.

TACC3 is not a centrosomal adaptor for ch-TOG

While TACC3 can be thought of as an adaptor in the context of TACC3–ch-TOG–clathrin, there is no evidence that it is an adaptor at centrosomes. It is clear that ch-TOG has a centrosomal distribution in interphase and mitosis (Fig 4A) [17, 33-35]. This localization persists in the absence of TACC3 [17, 33]. By contrast, in *Drosophila*, D-TACC – the sole TACC3 homolog – is apparently required to localize minispindles to centrosomes [36]. Is it possible that in human cells, TACC proteins can act as centrosomal adaptors for ch-TOG? To address this question, we sought a ch-TOG mutant that cannot bind to the TACC domain of TACC3 and tested whether this mutant is deficient in centrosomal localization.

We first narrowed down the TACC3-binding region within ch-TOG by testing for co-precipitation of recombinant ch-TOG fragments with a His-NusA tagged TACC3 fragment (629-838) using His-NusA as a control. Binding of ch-TOG(1517-1957) but not of ch-TOG(1517-1932) was observed suggesting that the region of ch-TOG that mediates binding is residues 1932-1957 (Fig 5A). Alignment of these regions from ch-TOG orthologs highlighted a conserved patch including a pair of leucines which we targeted for mutation (Fig 5B). Mutation of either L1939 or L1942 to either alanine or arginine blocked the ability of ch-TOG(1517-1957) to co-precipitate TACC3(629-838) (Fig 5C). Circular dichroism spectra of the L1939A and L1942A mutant proteins were similar to that of wild type ch-TOG(1517-1957) suggesting that these mutations had no significant effect on folding (Fig 5D).

We next introduced both mutations into ch-TOG to test if ch-TOG can bind the centrosome independently of TACC3. The ch-TOG-GFP(LL1939,1942AA) construct was expressed in ch-TOG-depleted HeLa cells and its subcellular distribution studied by confocal microscopy. Wild type ch-TOG-GFP was localized to kinetochores, spindle MTs and centrosomes (Fig 5E), whereas the mutant was not associated with spindle MTs, as expected but still localized to the centrosomes and kinetochores. In addition, the mutant tracked the plus-ends of MTs in interphase (Fig 5F), further confirming that +TIP

tracking of ch-TOG is not via TACC3. The kinetochore localization of ch-TOG has not been reported previously although Alp14, the *S. pombe* homolog of ch-TOG, localizes at kinetochores [32, 37]. This pool of ch-TOG is not readily detected by immunofluorescence [17], suggesting that it is inaccessible to antibodies directed against the C-terminus of ch-TOG.

These results suggest that the centrosomal localization of ch-TOG is indeed independent of TACC3 and also describe the molecular details of the TACC3–ch-TOG interaction. It is unclear why TACC3 is unable to bind ch-TOG at centrosomes and kinetochores. It could be that TACC3 is prevented from doing so because ch-TOG is in a different conformation or that it is bound to another protein. These are interesting questions for future study.

Summary

We have defined a new function of TACC3 as a +TIP at the very distal plus-end of the MT together with ch-TOG. This tracking occurs ahead of EB proteins and is distinct from the role TACC3 plays in concert with clathrin, regulated by Aurora-A kinase, as an adaptor for ch-TOG on kinetochore MTs.

TACC3 +TIP activity is evident in interphase where it is proposed to be important for cell migration. This is important because TACC3 is frequently overexpressed in various cancers where it correlates with an aggressive malignant phenotype and poor clinical outcome [29]. The potential for TACC3–ch-TOG +TIP activity to influence the speed of cell migration is interesting given that proteins that are involved in cell adhesion such as ENAH and VASP have previously been identified as TACC3 partners [20]. Moreover, the same study identified SLAIN2 and GTSE1 as TACC3 binding partners, both of which were subsequently shown to have +TIP activity and roles in cell migration [4, 38].

The +TIP activity in mitosis requires further investigation. We predict that it is involved in acentrosomal MT assembly during prometaphase [23]. The other recently described role for TACC3 in anaphase MT sliding [22] is dependent on Aurora-A kinase activity and so likely involves the TACC3–ch-TOG–clathrin pool rather than the TACC3–ch-TOG +TIP activity. Separating these two pools in mitosis will be key to understanding the two functions of TACC3 at this cell cycle stage.

Methods

Cell culture

HeLa cells (HPA/ECACC #93021013) were maintained in Dulbecco's Modified Eagle's Medium (DMEM) plus 10% fetal bovine serum (FBS) and 100 U/ml penicillin/streptomycin. HeLa Kyoto cells stably transfected with a BAC to express human TACC3 with a C-terminal GFP tag [20] were a kind gift from Tony Hyman (Dresden). Two lines were used MCP_ky_179 and 190, with identical results and were maintained in the same way as regular HeLa. RPE1 cells stable expressing EB3-tdTomato [39], were a kind gift from Anne Straube (Warwick). RPE1 cells were cultured in DMEM/Nutrient Mixture F-12 Ham (Sigma) supplemented with 10% FBS and 100 U/ml penicillin/streptomycin, 2 mM L-Glutamine and 0.25% Sodium bicarbonate (Sigma). RPE1 stably expressing EB3-tdTomato were maintained in medium containing 500 μg/ml G418. All cells were cultured at 37°C and 5% CO_2 in humidified incubator. HeLa and RPE1 cells were transfected using GeneJuice (Novagen) and FuGENE 6 (Promega) respectively and Lipofectamine2000 (Life Technologies) was used for transfection of siRNA. Transfections were carried out according to manufacturer's instructions in all cases.

Molecular Biology

Most plasmids were available from previous work [11, 17, 40]. To deplete endogenous ch-TOG and re-express ch-TOG-GFP, an existing plasmid (pBrain-GFP-ch-TOGKDP-shch-TOG) was modified to move the GFP from the N-terminus of ch-TOG to the C-terminus. This plasmid was subjected to site-directed mutagenesis to introduce LL1939,1942AA mutations. The target sequence for TACC3 siRNA was cagtttggaacttcctcgt (SASI_Hs01_00156991 MISSION pre-designed siRNA). Constructs for recombinant expression of TACC3(629-838) and ch-TOG truncates were produced as previously described [11]. Point mutations were introduced in pETM6T1 ch-TOG(1517-1957) by the Quikchange procedure (Stratagene).

Microscopy and analysis

For live cell imaging, cells were plated in 35 mm glass bottom fluorodishes. After 48 h after transfection cells were placed in a 37°C chamber on the microscope stage of a spinning disc confocal system (Ultraview Vox, Perkin Elmer) cultured in the CO2-independent media Leibovitz's L-15 Medium (Sigma) supplemented as for growth conditions. Imaging was performed using a 100X ~1.4 NA oil immersion objective lens. Cells were typically imaged every second for 1 minute. Cells were excited at 488 nm and 561 nm and images captured simultaneously with two cameras (Hamamatsu C10600-10B ORCA-R2). On the day of imaging, camera alignment was performed using 0.5 μm diameter fluorescent beads.

For FRAP experiments, HeLa cells were transfected with GFP-Tubulin and mCherry-TACC3, mCherry-LCa or Cherry-TACC3 LL[566,567]AA and FRAP was performed after 48 h using the FRAP module for Volocity. Fluorescence intensity of the photobleached ROI (I_{FRAP}), an unbleached ROI in the spindle (I_{ref}) and the background intensity (I_{bg}) was determined using Fiji/ImageJ. Corrected intensity was calculated using the equation.

$$I(t) = \frac{I_{FRAP}(t) - I_{bg}(t)}{I_{ref}(t) - I_{bg}(t)}$$

For fitting, I(t) was normalized using the equation:

$$I_{norm}(t) = \frac{I(t) - I(postbleach)}{I(0) - I(postbleach)}$$

The fraction of the starting fluorescence is therefore scaled such that the bleach gives I=0. GFP-Tubulin was used to control for the amount of MTs in the ROI. This fluorescence was monitored in parallel and cells with non-stable intensities in the FRAP region were discarded. Data from 10 cells from >3 independent experiments were averaged and fitted using a double exponential function (IgorPro 6.34, Wavemetrics).

$$I_{norm}(t) = y_0 + A_1 e^{(-\tau_1 t)} + A_2 e^{(-\tau_2 t)}$$

For knocksideways experiments, HeLa cells were transfected with pBrain-GFP-FKBP-TACC3KDP-shTACC3 (depletes endogenous TACC3 and re-expresses tagged TACC3) and pMito-PAGFP-FRB ('invisible' MitoTrap). Cells were treated with rapamycin (R8781, Sigma Aldrich) at 200 nM or DMSO 0.1% (control) for 20 min at 37°C. Cells were fixed in methanol at -20°C for 5 min, before immunostaining with mouse anti-EB1 (1:500, BD Transduction Laboratories, 610534) or rabbit anti-ch-TOG (1:5000, Autogen Bioclear, 34032) and Alexa568 conjugated secondary antibodies. Images were taken on a Nikon Ti epifluorescence microscope with 60X oil immersion objective (1.4 NA) and a Hamamatsu Orca-ER camera.

For immunofluorescence, cells were fixed with PTEMF (50 mM Pipes, pH 7.2, 10 mM EGTA, 1mM $MgCl_2$, 0.2% Triton X-100, and 4% paraformaldehyde) for 15 min at RT, and then permeabilized (PBS/0.1% Triton X-100) for 10 min. Cells were blocked (PBS, 3% BSA, and 5% goat serum) for 1 h, and then incubated for 1 h with the specified primary antibodies: mouse anti-CHC (X22, 1:1000), mouse anti-TACC3 (AbCam ab56595, 1:1000), rabbit anti-Pericentrin (Abcam ab4448, 1:5000). Secondary antibodies, Alexa Fluor 488 and 568 (Life Technologies, 1:500). Cells were rinsed with PBS and mounted with mowiol containing DAPI. Images were taken using a spinning disk confocal with a 60X objective and a z-step of 0.5 μm.

For migration analysis, RPE1 cells were seeded into Lab-Tek dishes (Nunc) coated with 10 µg/ml fibronectin (Sigma). On the day of imaging, nuclei were stained with NucRed™ Live 647 (R37106, Life technologies) and then imaged for 6 h at a rate of one image every 6 min or 20 min. Imaging was done using

a Nikon Ti microscope and Hamamatsu Orca-ER camera, using a 20X air objective. Cell movements were tracked using the Manual Tracking plug-in in Fiji/ImageJ to monitor the xy position of the centre of the nucleus. 2D Coordinates were fed to IgorPro for further analysis using custom-written procedures. A code snippet for rotation of a 2D set of co-ordinates about the origin is deposited at http://www.igorexchange.com/node/5895

Kymographs and temporal color-coded images of movies were generated in ImageJ. Images were cropped in ImageJ or Photoshop and figures were assembled in Illustrator CS5.1. Box plots show the median, 75th and 25th percentile and whiskers show 90th and 10th percentile.

Biochemistry

A rabbit polyclonal antibody was raised against peptides, EVIEGYRKNEESLKKC and TVEQKTKENEELTRIC to recognize the TACC domain of TACC3 (Eurogentec). Expression and purification of recombinant TACC3(629-838) and ch-TOG truncates was carried out as stated in earlier work [11]. *In vitro* binding assays between TACC3(629-838) and ch-TOG truncates were performed as previously stated [11]. For CD spectroscopy, wild type and point mutants of ch-TOG(1517-1957) were dialyzed into 20 mM sodium phosphate pH 7.0, 50 mM NaCl and diluted to 0.1 mg/ml. Spectra were collected on a Chirascan+ instrument (Applied Photophysics) using a 0.01 cm pathlength quartz cell at 20°C and are shown as the average of three replicates after baseline subtraction and smoothing. ClustalW2 was used to align ch-TOG sequences [41].

Acknowledgements

We thank Rachel Jones for technical assistance, Anne Straube (Warwick Medical School) and Tony Hyman (MPI Dresden) for important reagents, Fanni Gergely (Cancer Research UK Cambridge Institute) for help in designing antigen peptides for the production of the TACC3 TACC domain antibody and Mark Richards (University of Leicester; Cancer Research UK Leicester Centre) for assistance with CD spectroscopy. Colleagues at Warwick and Leicester provided important critical discussion. SJR is a Senior Cancer Research Fellow for Cancer Research UK (C25425/A15182). RB acknowledges funding from Cancer Research UK (C24461/A12772).

References

1. Desai A, Mitchison TJ (1997) Microtubule polymerization dynamics. *Annu Rev Cell Dev Biol* **13:** 83-117
2. Akhmanova A, Steinmetz MO (2010) Microtubule +TIPs at a glance. *J Cell Sci* **123:** 3415-3419
3. Mimori-Kiyosue Y, Shiina N, Tsukita S (2000) The dynamic behavior of the APC-binding protein EB1 on the distal ends of microtubules. *Curr Biol* **10:** 865-868
4. van der Vaart B *et al* (2011) SLAIN2 links microtubule plus end-tracking proteins and controls microtubule growth in interphase. *J Cell Biol* **193:** 1083-1099
5. Honnappa S *et al* (2009) An EB1-binding motif acts as a microtubule tip localization signal. *Cell* **138:** 366-376
6. Jiang K *et al* (2012) A Proteome-wide screen for mammalian SxIP motif-containing microtubule plus-end tracking proteins. *Curr Biol* **22:** 1800-1807
7. Nakamura S, Grigoriev I, Nogi T, Hamaji T, Cassimeris L, Mimori-Kiyosue Y (2012) Dissecting the nanoscale distributions and functions of microtubule-end-binding proteins EB1 and ch-TOG in interphase HeLa cells. *PLoS One* **7:** e51442
8. Maurer SP, Cade NI, Bohner G, Gustafsson N, Boutant E, Surrey T (2014) EB1 accelerates two conformational transitions important for microtubule maturation and dynamics. *Curr Biol* **24:** 372-384
9. Zanic M, Widlund PO, Hyman AA, Howard J (2013) Synergy between XMAP215 and EB1 increases microtubule growth rates to physiological levels. *Nat Cell Biol* **15:** 688-693
10. Thakur HC *et al* (2013) Role of centrosomal adaptor proteins of the TACC family in the regulation of microtubule dynamics during mitotic cell division. *Biol Chem* **394:** 1411-1423
11. Hood FE, Williams SJ, Burgess SG, Richards MW, Roth D, Straube A, Pfuhl M, Bayliss R, Royle SJ (2013) Coordination of adjacent domains mediates TACC3-ch-TOG-clathrin assembly and mitotic spindle binding. *J Cell Biol* **202:** 463-478
12. Thakur HC *et al* (2014) The centrosomal adaptor TACC3 and the microtubule polymerase chTOG interact via defined C-terminal subdomains in an Aurora-A kinase-independent manner. *J Biol Chem* **289:** 74-88
13. Kinoshita K, Noetzel TL, Pelletier L, Mechtler K, Drechsel DN, Schwager A, Lee M, Raff JW, Hyman AA (2005) Aurora A phosphorylation of TACC3/maskin is required for centrosome-dependent microtubule assembly in mitosis. *J Cell Biol* **170:** 1047-1055
14. Barr AR, Gergely F (2008) MCAK-independent functions of ch-Tog/XMAP215 in microtubule plus-end dynamics. *Mol Cell Biol* **28:** 7199-7211
15. LeRoy PJ, Hunter JJ, Hoar KM, Burke KE, Shinde V, Ruan J, Bowman D, Galvin K, Ecsedy JA (2007) Localization of human TACC3 to mitotic spindles is mediated by phosphorylation on Ser558 by Aurora A: a novel pharmacodynamic method for measuring Aurora A activity. *Cancer Res* **67:** 5362-5370
16. Cheeseman LP, Booth DG, Hood FE, Prior IA, Royle SJ (2011) Aurora A kinase activity is required for localization of TACC3/ch-TOG/clathrin inter-microtubule bridges. *Commun Integr Biol* **4:** 409-412
17. Booth DG, Hood FE, Prior IA, Royle SJ (2011) A TACC3/ch-TOG/clathrin complex stabilises kinetochore fibres by inter-microtubule bridging. *EMBO J* **30:** 906-919
18. Fu W, Tao W, Zheng P, Fu J, Bian M, Jiang Q, Clarke PR, Zhang C (2010) Clathrin recruits phosphorylated TACC3 to spindle poles for bipolar spindle assembly and chromosome alignment. *J Cell Sci* **123:** 3645-3651

19. Lin CH, Hu CK, Shih HM (2010) Clathrin heavy chain mediates TACC3 targeting to mitotic spindles to ensure spindle stability. *J Cell Biol* **189:** 1097-1105
20. Hubner NC, Bird AW, Cox J, Splettstoesser B, Bandilla P, Poser I, Hyman A, Mann M (2010) Quantitative proteomics combined with BAC TransgeneOmics reveals in vivo protein interactions. *J Cell Biol* **189:** 739-754
21. Cheeseman LP, Harry EF, McAinsh AD, Prior IA, Royle SJ (2013) Specific removal of TACC3/ch-TOG/clathrin at metaphase deregulates kinetochore fiber tension. *J Cell Sci* **126:** 2102-2113
22. Lioutas A, Vernos I (2013) Aurora A kinase and its substrate TACC3 are required for central spindle assembly. *EMBO Rep* **14:** 829-836
23. Fu W *et al* (2013) Self-assembly and sorting of acentrosomal microtubules by TACC3 facilitate kinetochore capture during the mitotic spindle assembly. *Proc Natl Acad Sci U S A* **110:** 15295-15300
24. Hood FE, Royle SJ (2011) Pulling it together: The mitotic function of TACC3. *Bioarchitecture* **1:** 105-109
25. Al-Bassam J, Chang F (2011) Regulation of microtubule dynamics by TOG-domain proteins XMAP215/Dis1 and CLASP. *Trends Cell Biol* **21:** 604-614
26. Widlund PO, Stear JH, Pozniakovsky A, Zanic M, Reber S, Brouhard GJ, Hyman AA, Howard J (2011) XMAP215 polymerase activity is built by combining multiple tubulin-binding TOG domains and a basic lattice-binding region. *Proc Natl Acad Sci U S A* **108:** 2741-2746
27. Nakagawa H, Koyama K, Murata Y, Morito M, Akiyama T, Nakamura Y (2000) EB3, a novel member of the EB1 family preferentially expressed in the central nervous system, binds to a CNS-specific APC homologue. *Oncogene* **19:** 210-216
28. Gergely F, Karlsson C, Still I, Cowell J, Kilmartin J, Raff JW (2000) The TACC domain identifies a family of centrosomal proteins that can interact with microtubules. *Proc Natl Acad Sci U S A* **97:** 14352-14357
29. Ha GH, Park JS, Breuer EK (2013) TACC3 promotes epithelial-mesenchymal transition (EMT) through the activation of PI3K/Akt and ERK signaling pathways. *Cancer Lett* **332:** 63-73
30. Gergely F, Kidd D, Jeffers K, Wakefield JG, Raff JW (2000) D-TACC: a novel centrosomal protein required for normal spindle function in the early Drosophila embryo. *Embo J* **19:** 241-252
31. Peset I, Seiler J, Sardon T, Bejarano LA, Rybina S, Vernos I (2005) Function and regulation of Maskin, a TACC family protein, in microtubule growth during mitosis. *J Cell Biol* **170:** 1057-1066
32. Sato M, Vardy L, Angel Garcia M, Koonrugsa N, Toda T (2004) Interdependency of fission yeast Alp14/TOG and coiled coil protein Alp7 in microtubule localization and bipolar spindle formation. *Mol Biol Cell* **15:** 1609-1622
33. Gergely F, Draviam VM, Raff JW (2003) The ch-TOG/XMAP215 protein is essential for spindle pole organization in human somatic cells. *Genes Dev* **17:** 336-341
34. Charrasse S, Schroeder M, Gauthier-Rouviere C, Ango F, Cassimeris L, Gard DL, Larroque C (1998) The TOGp protein is a new human microtubule-associated protein homologous to the Xenopus XMAP215. *J Cell Sci* **111 (Pt 10):** 1371-1383
35. Foraker AB, Camus SM, Evans TM, Majeed SR, Chen CY, Taner SB, Correa IR, Jr., Doxsey SJ, Brodsky FM (2012) Clathrin promotes centrosome integrity in early mitosis through stabilization of centrosomal ch-TOG. *J Cell Biol* **198:** 591-605
36. Lee MJ, Gergely F, Jeffers K, Peak-Chew SY, Raff JW (2001) Msps/XMAP215 interacts with the centrosomal protein D-TACC to regulate microtubule behaviour. *Nat Cell Biol* **3:** 643-649

37. Garcia MA, Vardy L, Koonrugsa N, Toda T (2001) Fission yeast ch-TOG/XMAP215 homologue Alp14 connects mitotic spindles with the kinetochore and is a component of the Mad2-dependent spindle checkpoint. *EMBO J* **20:** 3389-3401
38. Scolz M *et al* (2012) GTSE1 is a microtubule plus-end tracking protein that regulates EB1-dependent cell migration. *PLoS One* **7:** e51259
39. Theisen U, Straube E, Straube A (2012) Directional persistence of migrating cells requires Kif1C-mediated stabilization of trailing adhesions. *Dev Cell* **23:** 1153-1166
40. Royle SJ, Bright NA, Lagnado L (2005) Clathrin is required for the function of the mitotic spindle. *Nature* **434:** 1152-1157
41. Larkin MA *et al* (2007) Clustal W and Clustal X version 2.0. *Bioinformatics* **23:** 2947-2948
42. Shannon KB, Canman JC, Ben Moree C, Tirnauer JS, Salmon ED (2005) Taxol-stabilized microtubules can position the cytokinetic furrow in mammalian cells. *Mol Biol Cell* **16:** 4423-4436
43. Amaro AC, Samora CP, Holtackers R, Wang E, Kingston IJ, Alonso M, Lampson M, McAinsh AD, Meraldi P (2010) Molecular control of kinetochore-microtubule dynamics and chromosome oscillations. *Nat Cell Biol* **12:** 319-329

Figure Legends

Figure 1. TACC3 is a +TIP that tracks plus-ends of microtubules ahead of EB3.

(A) Single frames from live-cell imaging experiments of RPE1 cells expressing GFP-TACC3 in interphase and mitosis. RPE1 cells were stably expressing EB3-tdTomato. Similar results were seen in the parental RPE1 cell line. For each condition, a single frame from the movie (1 Hz) is shown together with kymographs to illustrate the movement of TACC3 comets over time. A representative MT shrinkage event is marked by a green arrow.

(B) Single frame (left) and color projection of live cell images of HeLa Kyoto cells with stably integrated BAC transgene to express TACC3-GFP under its native promoter. Late anaphase cells were imaged at 0.5 Hz and nine consecutive frames were projected into one image using different colors as indicated. Numbers indicate time (s). Scale bar, 10 µm (20 µm for interphase) and 10 s.

Figure 2. TACC3 +TIP activity is via its interaction with ch-TOG and separate from the TACC3–ch-TOG–clathrin inter-MT bridge complex.

(A) Single frame and color projection of live-cell imaging of TACC3-depleted HeLa cells expressing mCherry-tubulin (red) and RNAi-resistant GFP-TACC3, a non-phosphorylatable mutant (S558A) or a mutant that cannot bind clathrin (LL566,567AA), mutants that do not interact with ch-TOG (Δ678-681, Δ682-688). Cells in interphase or anaphase together with typical kymographs are shown (right). Scale bar, 20 *µ*m and 10 s.

(B) Representative micrographs of a knocksideways experiment to test for co-rerouting of EB1 or ch-TOG with TACC3. HeLa cells expressing GFP-FKBP-TACC3 and PAGFP-MitoTrap (not shown) were treated as indicated and fixed with methanol before staining with anti-EB1 or anti-ch-TOG. Scale bar, 10 *µ*m.

Figure 3. Role for TACC3 in cell migration.

(A) Overlay of individual tracks (nuclear position over time) of RPE1 cells transfected with siRNA targeting GL2 (siGL2, red) or TACC3 (siTACC3, blue). Tracks were aligned to the origin.

(B) Plots to show cumulative distance as a function of time for the tracks shown in A. N_{cell} = 147 (GL2), 154 (TACC3), from a single experiment.

(C) Overlay of individual tracks to assess directionality. Tracks from A were rotated so that the end point of each track aligned with the origin along the x-axis.

(D) Plot of cumulative distance as a function of displacement. Displacement is the Euclidian distance from the origin to the endpoint. Gradients of the lines of best fit were 0.81 (siGL2) and 0.79 (siTACC3).

(E) Box plot to show the speed of migration for the tracks shown.

(F) Box plot to show the relative speed of TACC3-depleted RPE1 cells versus control cells over three independent experiments. P values derived from Student's t-test are shown in D-F.

Figure 4. Distinct combinatorial pools of TACC3, ch-TOG and clathrin.

(A) Typical confocal micrographs to show the subcellular distributions of TACC3, ch-TOG and clathrin in mitotic (left) and interphase (right) HeLa cells. Untransfected cells were fixed and stained for pericentrin and either TACC3 or clathrin heavy chain, or in the case of ch-TOG, were transfected to express ch-TOG-GFP on a background of ch-TOG depletion and then fixed and stained for pericentrin (green in merge). Note the lack of colocalization of TACC3 and pericentrin in surrounding cells. For mitotic cells a single plane of a z-stack is shown. For interphase cells, a maximum intensity z-projection is shown. Zoomed regions show comparable magnification (2X and 4X for mitotic and interphase respectively). Scale bar, 10 μm.

(B) Bar chart to show the percentage of interphase cells with TACC3 in the vicinity of pericentrin staining (yellow) or no detectable enrichment (green). Results are shown for cells with one or two pericentrin puncta as indicated.

(C) Single confocal image to show an interphase cell that had TACC3 in the vicinity of centrosomes. Right, 3X enlargements of the centrosomal regions. Scale bar, 10 μm.

(D, E) The cellular pools of TACC3, ch-TOG and clathrin alone or in their possible combinations are shown for a model cell in mitosis (D) or interphase (E). Cytoplasmic populations of each protein can exchange with the corresponding pools and are not shown.

(F) Nanoscale model of a MT to show the conformation and approximate location of the two MT-resident pools. The complex of TACC3–ch-TOG binds to the distal tip of the MT. Recognition of the tip is by ch-TOG, which occurs in an autonomous manner. EB proteins can bind in a zone 30-60 nm away [8, 9]. Beyond this, TACC3–ch-TOG–clathrin complexes can bind. TACC3 is active in binding, but only in partnership with clathrin [11]. The full clathrin triskelion and cross-bridges to other MTs are not shown for simplicity.

Figure 5. A ch-TOG mutant deficient in TACC binding localizes to centrosomes and tracks the plus-ends of MTs.

(A) Co-precipitation assay between His-NusA-TACC3(629-838) and fragments of the C-terminal region of ch-TOG. His-NusA-TACC3(629-838) was bound to Ni Sepharose beads and incubated with ch-TOG proteins. His-NusA was used as a tag binding control.

(B) Sequence alignment of the TACC3-binding region of ch-TOG orthologs. Identical residues are represented with '*', conserved amino acids with ':' and semi-conserved residues with '.'. Leucine residues marked in red were targeted for mutation.

(C) Co-precipitation assay between wild type and point mutants of His-NusA-ch-TOG(1517-1957) and TACC3(629-838). His-NusA-ch-TOG(1517-1957) wild type and mutant proteins were bound to Ni Sepharose beads and then incubated with TACC3(629-838). His-NusA was used as a tag binding control. The reactions were separated by SDS-PAGE (above) and subject to Western blot using an anti-TACC3 TACC domain antibody (below). Input was 1/10 of the binding reaction for Coomassie and 1/50 for Western blot.

(D) Circular dichroism spectroscopy of wild type ch-TOG(1517-1957) and L1939A and L1942A mutants.

(E) Confocal micrographs of ch-TOG-depleted HeLa cells expressing ch-TOG-GFP wild type (left) or LL1939,1942AA double mutant (centre). Kymographs showing similar interphase plus-end tracking for wild type (WT) and LL1939,1942AA double mutant (Mut) ch-TOG-GFP (right).

Supplementary Information

The TACC3–ch-TOG–clathrin complex is highly dynamic

Previous work suggested that the TACC3–ch-TOG–clathrin complex is rapidly turned over at the mitotic spindle [14, 21]. In order to measure TACC3 dynamicity on MTs, we carried out fluorescence recovery after photobleaching (FRAP) experiments on mitotic cells expressing mCherry-TACC3 and GFP-tubulin (see Methods). Following photobleaching, mCherry-TACC3 fluorescence recovered almost completely (to ~93% of the prebleach level). Recovery was best fit by a double exponential function with A_{fast} = 15%, τ_{fast} = 1.4 s, A_{slow} 85% and τ_{slow} =18.4 s (Supplementary Figure 1 and Supplementary Table 1). To compare this with clathrin we carried out a similar analysis with mCherry-clathrin light chain a (mCherry-LCa). Recovery was complete with a larger fast component A_{fast} = 49%, τ_{fast} = 3.5 s, A_{slow} 51% and τ_{slow} = 21.9 s. Since there is a larger cytoplasmic pool of clathrin compared with TACC3, this suggests that the fast recovery component for both proteins that represents diffusion of cytoplasmic protein. The slow component, which had similar kinetics for both proteins, represents exchange of the pool of TACC3 and clathrin bound to the spindle.

Two further experiments, together with contemporaneous live-cell imaging of TACC3 dynamics (main paper) suggested that the slow component was actually composed of two distinct pools of TACC3 that turned over with equivalent kinetics. First, a mutant of TACC3 (LL566,567AA) that is unable to bind clathrin [11] recovered with a larger fast component, as expected. However, the slow component remained A_{fast} = 61%, τ_{fast} = 2.6 s, A_{slow} 39% and τ_{slow} = 28.9 s. We initially attributed this to incomplete depletion of endogenous TACC3 or partial blockade of the clathrin–TACC3 interaction. However, FRAP experiments using Taxol treatment of mitotic cells expressing wild type mCherry-TACC3 showed a partial recovery (~60%) with the following kinetics: A_{fast} = 5%, τ_{fast} = 1.3 s, A_{slow} 95% and τ_{slow} = 23 s. Taxol inhibits MT plus-end dynamics and causes the dissociation of +TIPs [42]. The increase in the immobile fraction suggests that the residence of TACC3 on the spindle had increased. Whereas the unaltered kinetics of the slow component suggests that another slow population is now unmasked, representing a distinct pool of TACC3 that turns over with similar kinetics. Together with the imaging data described in the main paper, these results suggested the following model. Three pools of TACC3 in mitotic cells; 1) fast fraction – cytoplasmic diffusion; 2) slow fraction A – TACC3 in complex with clathrin on the mitotic spindle. 3) slow fraction B – TACC3 binding to MTs with similar association/dissociation kinetics as slow fraction A (Supplementary Figure 1). The exchange of all pools of TACC3 is an order of magnitude faster than tubulin turnover at the spindle and the rate of poleward flux [43].

Supplementary Figure 1. Fluorescence recovery after photobleaching (FRAP) FRAP analysis of TACC3 dynamics in mitotic cells.

(A) Average FRAP traces for metaphase cells expressing the indicated mCherry-tagged construct. Plots show the mean ± s.e.m. fluorescence that is scaled to examine the recovery following photobleaching (see Methods). N = 10 cells. Recovery was best fit by a double exponential function (thick line).

(B) Stacked bar chart to show the proportion of recovery by fast (dark) and slow (light) processes. The bar indicates the scaled co-efficient, error bars are ± S.D. of the fitting procedure. Kinetic parameters for the fits are shown in Supplementary Table 1.

Supplementary Movie 1 A video of GFP-TACC3 expressed in an interphase RPE1 cell stably expressing EB1

Live-cell imaging was done using a spinning disk microscope with a 100X ~1.4 NA oil immersion objective lens. Images were captured every second for 1 minute (video playback is 10 fps). Cells were excited at 488 nm and 561 nm and images captured simultaneously with two cameras (Hamamatsu C10600-10B ORCA-R2). The same cell is shown in Figure 2A.

Supplementary Movie 2 A video of GFP-TACC3 expressed in a mitotic RPE1 cell stably expressing EB1

Live-cell imaging was done using a spinning disk microscope with a 100X ~1.4 NA oil immersion objective lens. Images were captured every second for 1 minute (video playback is 10 fps). Cells were excited at 488 nm and 561 nm and images captured simultaneously with two cameras (Hamamatsu C10600-10B ORCA-R2). The same cell is shown in Fig 1B.

Supplementary Movie 3 A video of a HeLa Kyoto cell in anaphase expressing TACC3-GFP under its endogenous promoter

Live-cell imaging was done using a spinning disk microscope with a 100X ~1.4 NA oil immersion objective lens. Images were captured every second for 1 minute (video playback is 10 fps). The same cell is shown in Fig 1C.

Supplementary Table 1 Kinetic parameters of curve fitting for FRAP experiments.

	Clathrin (LCa)	**TACC3**	**TACC3 + Taxol**	**TACC3 (LL566,567AA)**
Recovery (%)	1.08 (108.36)	0.93 (92.61)	0.59 (59.28)	0.9 (90.18)
A_1 (% of recovery)	-0.53 (49.19)	-0.14 (14.78)	-0.03 (5.00)	-0.55 (61.19)
τ_1 s	3.45 ± 0.15	1.36 ± 0.62	1.31 ± 1.07	2.55 ± 0.44
A_2 (% of recovery)	-0.54 (50.82)	-0.79 (85.24)	-0.56 (95.00)	-0.35 (38.81)
τ_2 s	21.90 ± 0.58	18.44 ± 0.65	22.95 ± 0.44	28.86 ± 6.14
$T_{1/2}$ s	5.282	9.87	14.74	3.43

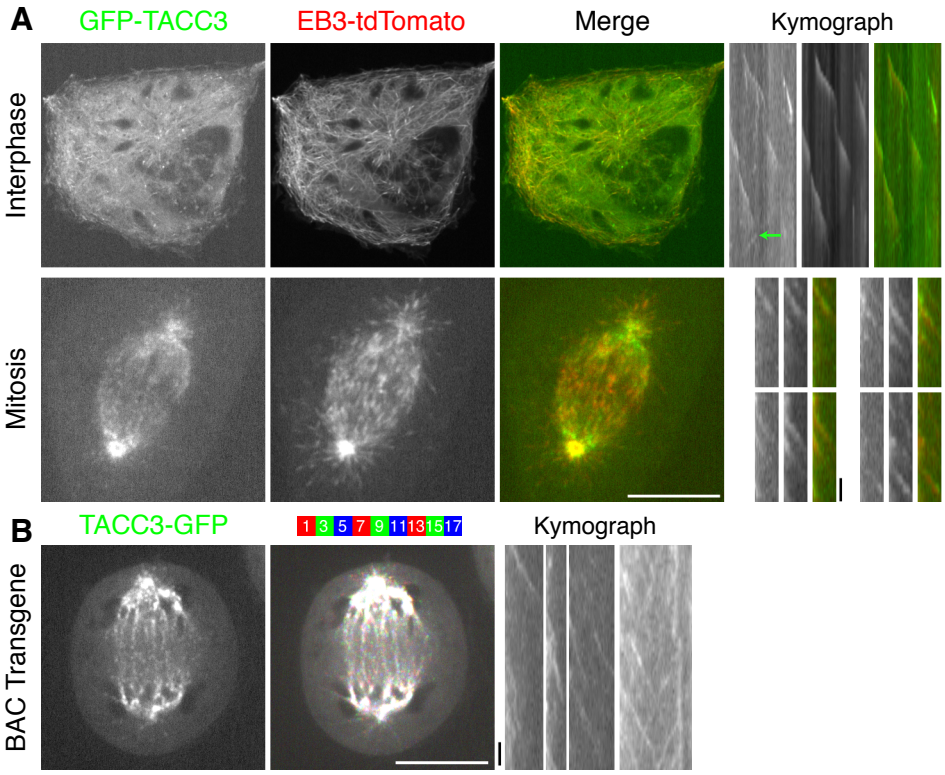
A
GFP-TACC3
EB3-tdTomato
Merge
Kymograph
Interphase
Mitosis
B
TACC3-GFP
1 3 5 7 9 11 13 15 17
Kymograph
BAC Transgene

Figure 1

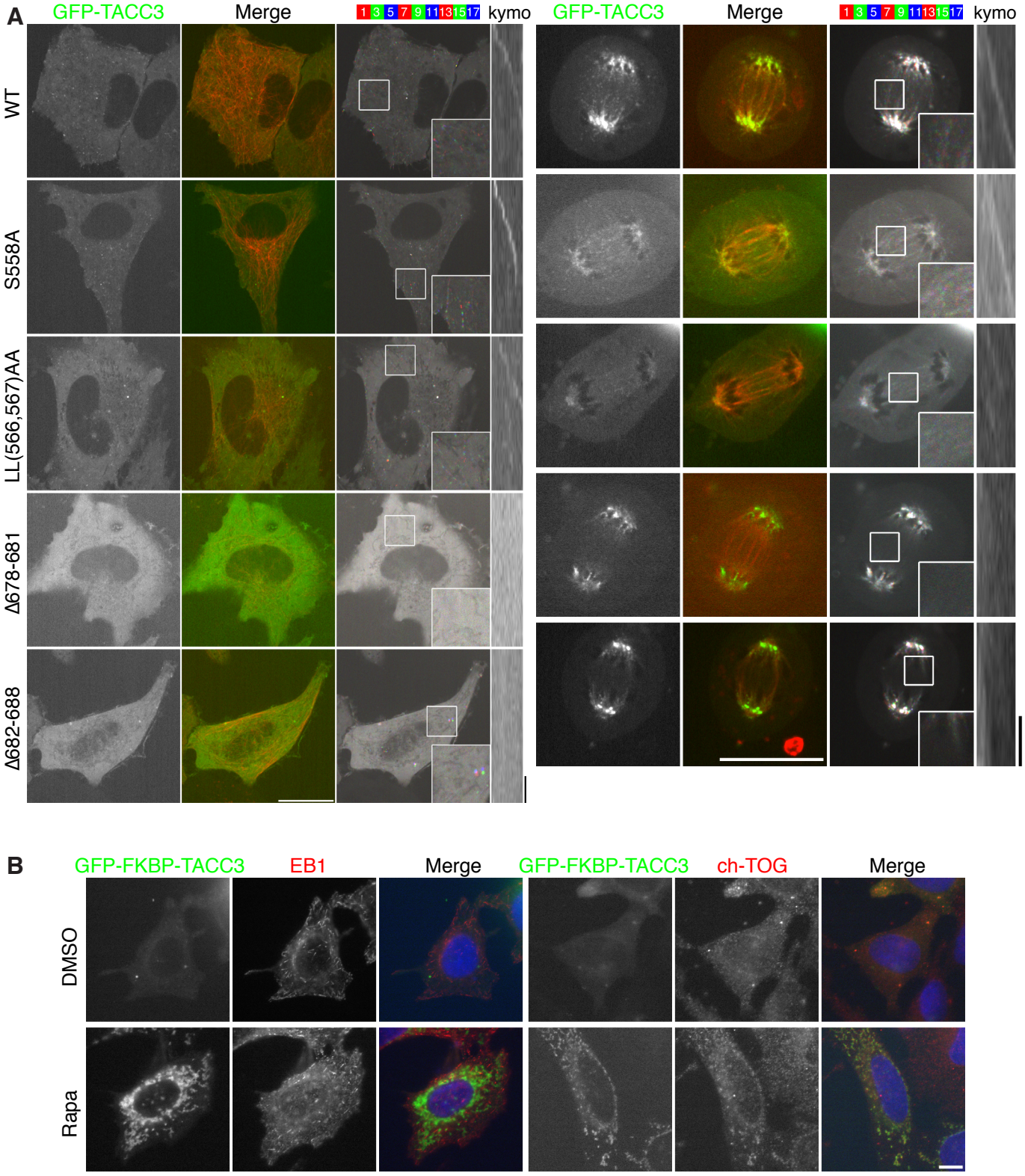
A
GFP-TACC3
Merge
1 3 5 7 9 11 13 15 17
kymo
WT
S558A
LL(566,567)AA
Δ678-681
Δ682-688
B
GFP-FKBP-TACC3
EB1
Merge
ch-TOG
DMSO
Rapa

Figure 2

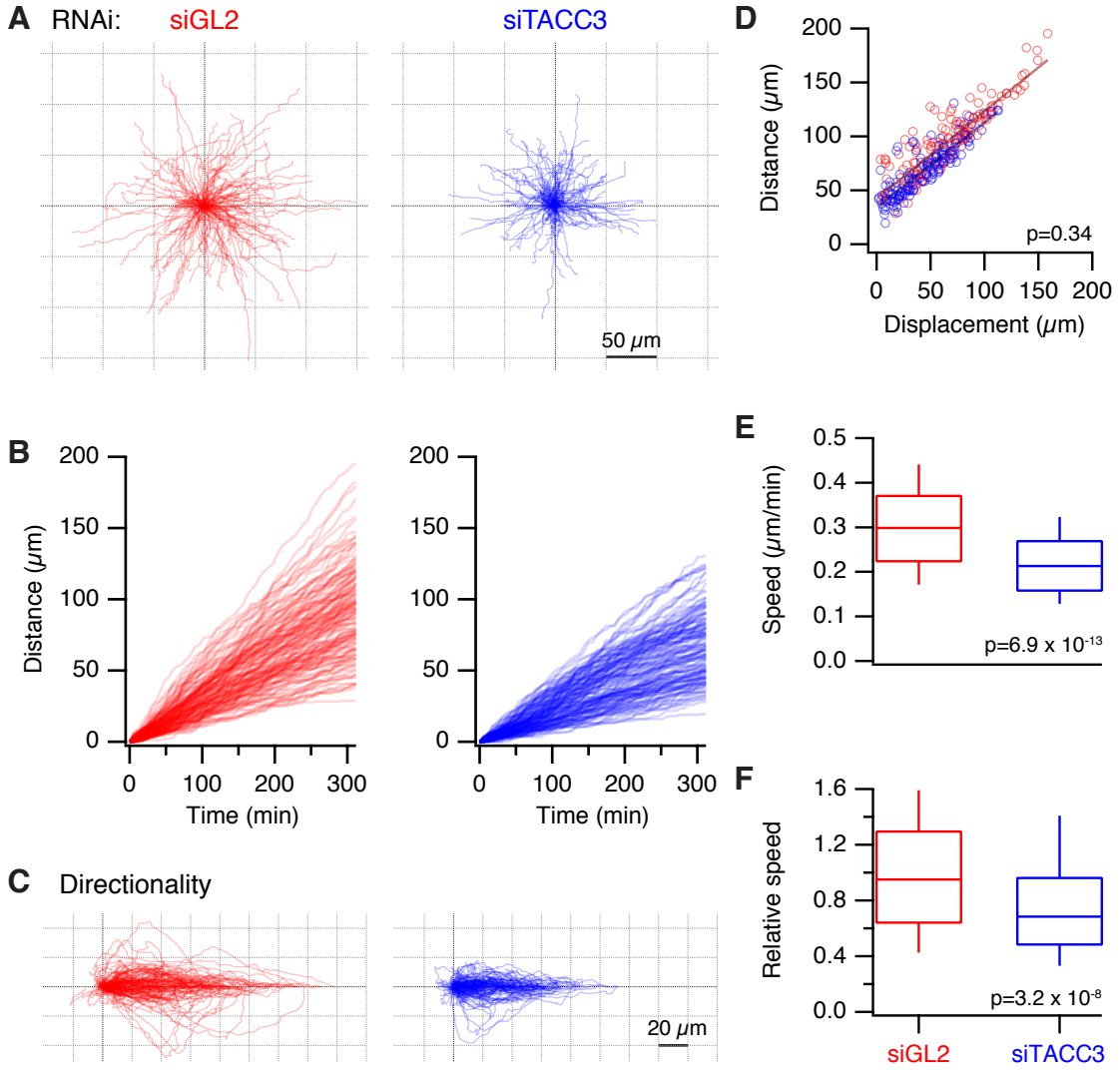
A
RNAi:
siGL2
siTACC3
50 μm
B
Distance (μm)
Time (min)
C
Directionality
20 μm
D
Distance (μm)
Displacement (μm)
p=0.34
E
Speed (μm/min)
p=6.9 x 10-13
F
Relative speed
p=3.2 x 10-8
siGL2
siTACC3

Figure 3

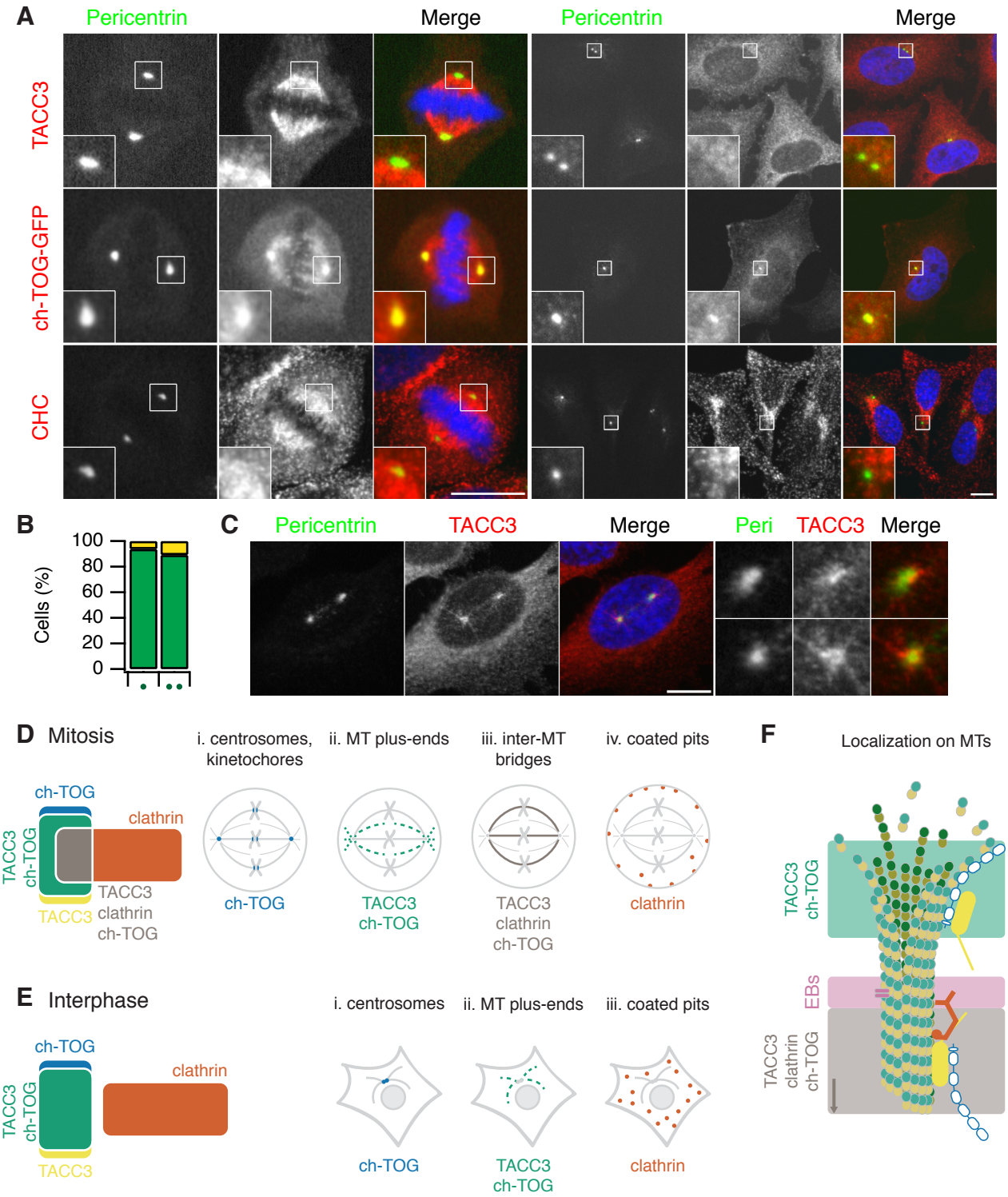
A
Pericentrin
Merge
Pericentrin
Merge
TACC3
ch-TOG-GFP
CHC
B
Cells (%)
100
80
60
40
20
0
C
Pericentrin
TACC3
Merge
Peri
TACC3
Merge
D Mitosis
i. centrosomes, kinetochores
ii. MT plus-ends
iii. inter-MT bridges
iv. coated pits
ch-TOG
clathrin
TACC3
ch-TOG
TACC3
TACC3
clathrin
ch-TOG
ch-TOG
TACC3
ch-TOG
TACC3
clathrin
ch-TOG
clathrin
E Interphase
i. centrosomes
ii. MT plus-ends
iii. coated pits
ch-TOG
clathrin
TACC3
ch-TOG
TACC3
ch-TOG
TACC3
ch-TOG
clathrin
F
Localization on MTs
TACC3
ch-TOG
EBs
TACC3
clathrin
ch-TOG

Figure 4

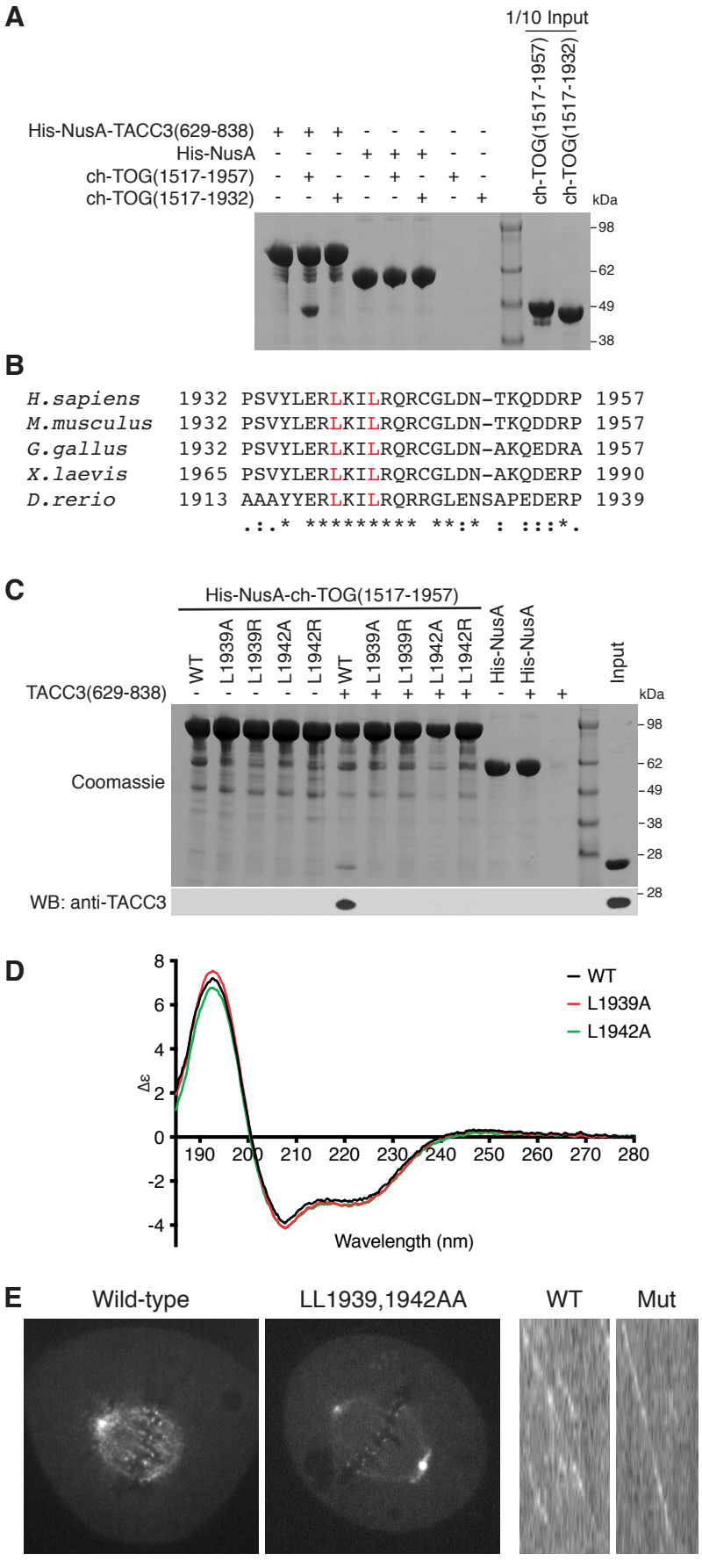
A
1/10 Input
ch-TOG(1517-1957)
ch-TOG(1517-1932)
His-NusA-TACC3(629-838) + + + - - - - -
His-NusA - - - + + + - -
ch-TOG(1517-1957) - + - - + - + -
ch-TOG(1517-1932) - - + - - + - +
kDa
98
62
49
38
B
H.sapiens 1932 PSVYLERLKILRQRCGLDN-TKQDDRP 1957
M.musculus 1932 PSVYLERLKILRQRCGLDN-TKQDDRP 1957
G.gallus 1932 PSVYLERLKILRQRCGLDN-AKQEDRA 1957
X.laevis 1965 PSVYLERLKILRQRCGLDN-AKQDERP 1990
D.rerio 1913 AAAYYERLKILRQRRGLENSAPEDERP 1939
.:.* ********* **:* : :::*.
C
His-NusA-ch-TOG(1517-1957)
WT
L1939A
L1939R
L1942A
L1942R
WT
L1939A
L1939R
L1942A
L1942R
His-NusA
His-NusA
Input
TACC3(629-838)
Coomassie
WB: anti-TACC3
kDa
98
62
49
38
28
28
D
WT
L1939A
L1942A
Δε
8
6
4
2
0
-2
-4
190
200
210
220
230
240
250
260
270
280
Wavelength (nm)
E
Wild-type
LL1939,1942AA
WT
Mut

Figure 5

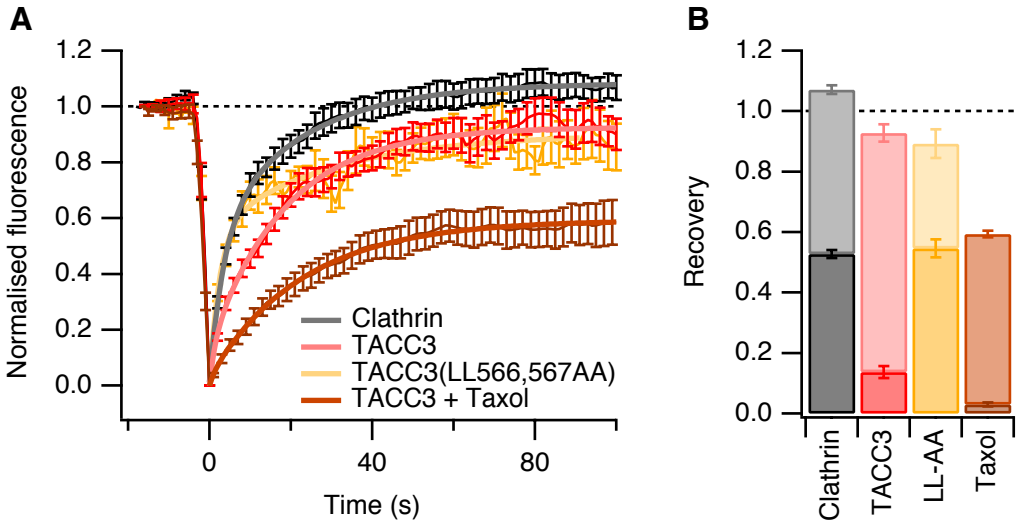

Supplementary Figure 1